JGR Atmospheres

RESEARCH ARTICLE
10.1029/2019JD030466

Direct Online Mass Spectrometry Measurements of Ice Nucleating Particles at a California Coastal Site

G. C. Cornwell[1,4], C. S. McCluskey[2,5], E. J. T. Levin[2], K. J. Suski[2,4], P. J. DeMott[2], S. M. Kreidenweis[2], and K. A. Prather[1,3]

[1]Department of Chemistry and Biochemistry, University of California, San Diego, CA, USA, [2]Department of Atmospheric Science, Colorado State University, Fort Collins, CO, USA, [3]Scripps Institution of Oceanography, University of California, San Diego, CA, USA, [4]Now at Pacific Northwest National Laboratory, Richland, WA, USA, [5]Now at National Center for Atmospheric Research, Boulder, CO, USA

Abstract The formation of ice in clouds can strongly impact cloud properties and precipitation processes during storms, including atmospheric rivers. Sea spray aerosol (SSA) particles are relatively inefficient as ice nucleating particles (INPs) compared to mineral dust. However, due to the vast coverage of the Earth's surface by the oceans, a number of recent studies have focused on identifying sources of marine INPs, particularly in regions lacking a strong influence from dust. This study describes the integration, validation, and application of a system coupling a continuous flow diffusion chamber with a single particle mass spectrometer using a pumped counterflow virtual impactor to remove nonnucleated particles and selectively measure the composition of INPs with a detection efficiency of 3.10×10^{-4}. In situ measurements of immersion freezing INP composition were made at a coastal site in California using the integrated system. Mineral dust particles were the most abundant ice crystal residual type during the sampling period and found to be ice active despite having undergone atmospheric processing. SSA were more abundant in ambient measurements but represented only a minor fraction of the ice crystal residual population at −31 °C. Notably, the SSA particles that activated were enriched with organic nitrogen species that were likely transferred from the ocean. Calculations of ice nucleation active site densities were within good agreement with previous studies of mineral dust and SSA.

Key Points:
- The most abundant immersion freezing ice nucleating particle type (T = −30 °C) was mineral dust during a week-long study at a coastal site
- Nitrate content made little difference to the ice nucleation activity of dust
- Sea spray aerosol that formed ice crystals were enriched in organic nitrogen species

Supporting Information:
- Supporting Information S1

Correspondence to:
K. A. Prather,
kprather@ucsd.edu

Citation:
Cornwell, G. C., McCluskey, C. S., Levin, E. J. T., Suski, K. J., DeMott, P. J., Kreidenweis, S. M., & Prather, K. A. (2019). Direct online mass spectrometry measurements of ice nucleating particles at a California coastal site. *Journal of Geophysical Research: Atmospheres*, *124*, 12,157–12,172. https://doi.org/10.1029/2019JD030466

Received 7 MAR 2019
Accepted 30 JUL 2019
Accepted article online 28 OCT 2019
Published online 19 NOV 2019

Author Contributions:
Conceptualization: P. J. DeMott, K. A. Prather
Data curation: C. S. McCluskey
Formal analysis: K. J. Suski
Funding acquisition: P. J. DeMott, S. M. Kreidenweis, K. A. Prather
Investigation: C. S. McCluskey, K. J. Suski
Methodology: G. C. Cornwell, C. S. McCluskey, E. J. T. Levin, K. J. Suski, P. J. DeMott
Project administration: S. M. Kreidenweis, K. A. Prather
Supervision: P. J. DeMott
Validation: G. C. Cornwell, C. S. McCluskey, E. J. T. Levin, K. J. Suski
Writing - original draft: K. J. Suski
Writing – review & editing: G. C. Cornwell, C. S. McCluskey, K. J. Suski, P. J. DeMott, K. A. Prather

1. Introduction

Atmospheric aerosol particles capable of initiating heterogeneous ice nucleation (IN), ice nucleating particles (INPs), are rare but play an important role in affecting the amount, type, and spatial distribution of precipitation (Fan et al., 2014; Fan et al., 2017; Ralph et al., 2016). Atmospheric rivers (ARs) are long and narrow storm systems which are typified by strong horizontal vapor transport (Zhu & Newell, 1998). ARs are particularly important in California, because two or three ARs can account for half of the state's annual water budget in addition to being responsible for flooding events on the west coast of the United States (Dettinger et al., 2011). INP formation and subsequent cloud microphysical processes are possible factors that have been hypothesized to positively affect precipitation totals in ARs (Ault et al., 2011). While local and long-range transported aerosols can be important sources of INPs, landfalling ARs also bring in marine and coastal air masses with their own distinct aerosol populations (Creamean et al., 2013) that have been hypothesized to affect the cloud and precipitation properties of these storms (Ralph et al., 2016). This study investigates the INP populations present in marine and coastal air masses that may influence ARs.

Previous studies of INPs in marine environments suggest that elevated INP concentrations could be correlated to regions of ocean water upwelling and high biological activity (Bigg, 1973; Schnell & Vali, 1976). These findings have been supported in laboratory studies of nascent marine INPs, in which increases in INP activity were observed during phytoplankton blooms (DeMott et al., 2016; McCluskey et al., 2017; McCluskey, Hill, et al., 2018) and in measurements of marine phytoplankton and exudates (Knopf et al., 2011; Wilson et al., 2015). Sea spray aerosol (SSA) composition is a complex mixture of inorganic salts, particulate organics (including bacteria and viruses), and organic matter found in the ocean (Cochran, Laskina, et al., 2017; Cochran, Ryder, et al., 2017). An observed increase in SSA IN-activity has been attributed to either microbes (McCluskey, Hill, et al., 2018) or surface-active molecules such as proteins or long-chain fatty acids (DeMott et al., 2018; McCluskey, Hill, et al., 2018; Wilson et al., 2015). McCluskey,

Ovadnevaite, et al. (2018) identified a period of elevated heat-labile INP concentrations in pristine marine air associated with elevated marine organic aerosol arising from the North Atlantic Ocean. Other measurements of INPs at coastal sites concluded that local terrestrial bioaerosol and dust were the major sources of INPs with little evidence for marine sources of INPs (Mason et al., 2015). INP measurements at a coastal site in the Arctic (Creamean et al., 2018) suggested that the major source of INPs were dust and primary marine aerosol, while shipborne measurements in the Arctic determined dust to be the primary contributor to INP concentrations (Irish et al., 2019). However, all of these studies lacked direct measurements that conclusively identified the composition of individual INPs.

Typically, 1 in 10^5 atmospheric particles in the free troposphere acts as an INP at −30 °C (DeMott et al., 2010). Therefore, bulk aerosol chemistry measurements are unable to provide insights into INP composition. In this study, we build upon previous studies that have devised a methodology to measure INP composition using single particle mass spectrometry (Corbin et al., 2012; Cziczo et al., 2003; DeMott et al., 2003; Gallavardin et al., 2008; Richardson et al., 2007). An aerosol time-of-flight mass spectrometer (ATOFMS), which provides real-time, size-resolved chemical composition of individual particles (Gard et al., 1997), was coupled to a continuous flow diffusion chamber (CFDC) which measures INP concentrations in real time by creating a cold, humid environment where INPs can nucleate into ice crystals (Rogers, 1988). In a CFDC, ice crystals are grown to exceed the sizes of other aerosols as the means of differentiating the numbers of INPs in a volume of air. Connecting the CFDC and ATOFMS with a pumped counterflow virtual impactor (PCVI), which separates particles on the basis of inertia (Kulkarni et al., 2011), allows for the selective measurement of ice crystal residuals (the INPs) without interference from non-INPs. To our knowledge, coupling a CFDC to a single particle mass spectrometer such as the ATOFMS to sample INP composition has not previously been attempted in a marine or coastal environment. While the INP population at the surface in coastal California is not necessarily expected to be representative of the INP population at the altitudes where clouds form, Creamean et al. (2013) showed that aerosol from the marine boundary layer can seed clouds during ARs and thus these aerosols may be important sources of INPs under certain conditions.

This paper describes the development and characterization of an integrated instrumental configuration for the real-time characterization of INPs. This technique was subsequently applied to investigate INP composition at the University of California, Davis Bodega Marine Laboratory, from 12–19 February 2015. The CFDC was operated in order to nucleate INPs through the immersion/condensation freezing mode, which is the most relevant IN mechanism for mixed-phase clouds such as those found in winter orographic storms in California. Instrument configurations, validation experiments, and the field campaign are detailed in section 2. Results from the validation experiments and field measurements are presented and discussed in section 3, while section 4 provides a short summary.

2. Materials and Methods

This work focuses upon integrating a CFDC with an ATOFMS and a PCVI to characterize INPs in both lab and field experiments. Here we provide a short overview of the materials and methods to clarify what was done. The operation and data analysis of the CFDC and the ATOFMS will be described in sections 2.1 and 2.2, respectively, while a description of the integration of the two instruments using a PCVI to isolate ice nucleating particles from unactivated particles and an overview of validation experiments are given in section 2.3 (results for these experiments are in section 3.1). Section 2.4 details the measurements taken at a coastal site in California during February 2015. Section 2.5 describes IN active site densities for dust and SSA using the integrated CFDC-PCVI-ATOFMS and an aerodynamic particle sizer (APS). Finally, section 2.6 discusses the uncertainties and associated with the measurements performed in this study.

2.1. CFDC Operation and Analysis

The Colorado State University (CSU) CFDC (Eidhammer et al., 2010; Rogers, 1988) was used to make real-time INP concentration measurements. The CSU-CFDC is a vertically mounted system with cylindrical walls 1.1 cm apart. The walls are chemically treated to be wettable by water, and each cylindrical column is independently temperature controlled. To form a thin layer of ice on each wall, the annular gap is flooded with water, while each wall is held at approximately −27 °C. After icing, aerosols are introduced into the annular gap via flow through a cylindrical knife edge inlet, which is surrounded by a dry, particle-free sheath flow. Both the knife edge and the sheath flow focus the minor aerosol flow into a lamina, where the

temperature and relative humidity with respect to water (RH_w) can be controlled by controlling the temperature of each cylindrical column. For immersion mode freezing experiments, the wall temperatures were set to a sample RH_w of nominally 105% to ensure that aerosol activates into droplets. Those droplets that contain INPs at the aerosol lamina temperature or warmer nucleate to form ice. The bottom third of the CSU-CFDC is the droplet-evaporation section, where the ice-coated walls are held at the same temperature. Here, the aerosol lamina adjusts toward ice saturation and is therefore water subsaturated. Thus, droplets will evaporate in this section and ice crystals will persist. All particles larger than ~500 nm are detected by an optical particle counter at the bottom of the evaporation section. Under the conditions in these experiments, ice crystals are assumed to be larger than 3.0 μm based on expected growth rates of ice particles and previous observations of the ice crystal size mode. The CFDC was operated for this study with a 1.5 μm (50% cutoff) impactor in front of the inlet in order to ensure that large aerosol particles were not erroneously counted as INPs.

Methods for accounting for CFDC measurement uncertainty and background follow previous work (Schill et al., 2016) and are summarized here. Number concentrations of INPs (N_{INPs}) and particles larger than 500 nm (N_{500}) were determined for 3–5 minute subsampling period within a given sampling period. Standard error associated with N_{INPs} and N_{500} were determined following Poisson counting statistics (Taylor, 1997). Periods between sampling were dedicated to measuring background concentrations by measuring filtered air. Background N_{INPs} and N_{500} were determined by calculating a time-weighted average of the filter periods before and after the sampling period. This value was subtracted from the sample N_{INPs} and N_{500}, and the standard errors were added in quadrature. Statistically significant N_{INPs} were defined herein as those that were higher than the background concentration plus two times the standard deviation.

An aerosol concentrator (Model 4240, MSP Corporation; Romay et al., 2002) was placed upstream of the CFDC to improve INP sampling statistics, as described in Tobo et al. (2013). Enhancements in aerosol concentrations are obtained in this concentrator using virtual impactors which affect only particles with diameters larger than 0.5 μm. In previous studies, the enhancement factor for aerosol particles varied from 40 at 0.5 microns up to about 140 at diameters above 1 μm (Tobo et al., 2013). Following Tobo et al. (2013), the INP concentration factor (ICF) for INPs was defined using the ratio of N_{INP} sampling with versus without the concentrator, as measured within 15 minutes before or after the 3–5 minute subsampling period. N_{INPs} measured without the concentrator were often not statistically significantly different from background concentrations, and the calculated ICFs were highly variable from day to day with an average and standard deviation of 7.7 ± 10.2. Therefore, an ICF was calculated for each subsampling period when possible (i.e., when N_{INP} were statistically significant), and a daily mean and standard deviation of ICF was used for other subsampling periods. Daily ICFs ranged from 1.2 to 22.9, lower than previous studies (e.g., 90 ± 3, Suski et al., 2018) due to changes in the concentrator performance experienced during this study. Standard error associated with the ICF was propagated in the final N_{INP}, calculated by dividing the subsample N_{INP} by the ICF.

2.2. ATOFMS Operation and Analysis

Size-resolved single particle mixing state was measured using an ATOFMS (Gard et al., 1997). Single particle mass spectra and size data were imported into MATLAB (The MathWorks, Inc.) and analyzed via the software toolkit FATES (Sultana, Al-Mashat, et al., 2017; Sultana, Cornwell, et al., 2017). Particles were divided into clusters based on their mass spectral features via an adaptive neural network and recombined based upon their characteristic mass spectra and size distributions (Rebotier & Prather, 2007; Song et al., 1999). Similar to previous field studies using ATOFMS analysis (Cahill et al., 2012; Pratt & Prather, 2010; Sullivan et al., 2007), particle types were manually regrouped upon inspection of the clusters based on spectral similarities. Particle type number, fraction, and standard error of measurement for each particle type are shown in Table 1, while representative spectra of the eight particle types detected in this study are shown in Figure 1. The characteristic ion markers for all types and assignments from the literature are given in Table 1.

2.3. Integration of the CFDC-PCVI-ATOFMS

Prior to the field study, initial optimization experiments integrating the CFDC and the ATOFMS with the PCVI were conducted prior to the field study at CSU in Fort Collins, CO. Block diagrams for the instrumental setup and the flow configuration are shown in Figure 2. The flows of the PCVI (Brechtel Manufacturing

Table 1
Description of ATOFMS Particle Types, Including Common Ion Marker Assignments and Literature References

Particle type	Characteristic ion markers
Dust	$^{7}Li^{+}$, $^{23}Na^{+}$, $^{27}Al^{+}$, $^{39}K^{+}$, $^{48,64}Ti,TiO^{+}$, $^{54,56}Fe^{+}$, $^{60}SiO_2^{-}$ $^{76}SiO_3^{-}$, $^{79}PO_3^{-}$ (Silva et al., 2000)
Na/K	$^{23}Na^{+}$, $^{39}K^{+}$ (Pratt & Prather, 2010).
Sea spray aerosol (SSA)	$^{23}Na^{+}$, $^{24}Mg^{+}$, $^{39}K^{+}$, $^{46}Na_2^{+}$, $^{81,83}Na_2Cl^{+}$, $^{35,37}Cl^{-}$, $^{46}NO_2^{-}$, $^{58}NaCl^{-}$, $^{62}NO_3^{-}$, $^{93,95,97}NaCl_2^{-}$ (Gard et al., 1998)
Primary biological (Bio)	Strong $^{39}K^{+}$ and $^{79}PO_3^{-}$, minor contributions from 59^{+}, 74^{+}, nucleoside fragment peaks at 66^{-}, 71^{-}, 90^{-} (Fergenson et al., 2004; Sultana, Al-Mashat, et al., 2017; Sultana, Cornwell, et al., 2017)
Elemental carbon (EC)	Clusters every 12 m/z at C_n^{+} and C_n^{-} (Moffet & Prather, 2009; Spencer & Prather, 2006)
Organic carbon (OC)	$^{27}C_2H_3^{+}$, $^{29}C_2H5$, $^{37}C_3H^{+}$, $^{43}CH_3CO^{+}$/$CHNO^{+}$ (Qin et al., 2012; P. Silva & Prather, 2000; Spencer & Prather, 2006)
Elemental carbon organic carbon (ECOC)	$^{12}C^{+}$, $^{24}C_2^{+}$, $^{27}C_2H_3^{+}$, $^{36}C_3^{+}$, $^{37}C_3H^{+}$, $^{43}CH_3CO^{+}$/$CHNO^{+}$ (Moffet & Prather, 2009; Qin et al., 2012)
Biomass burning (BB)	Intense $^{39}K^{+}$ and $^{97}HSO_4^{-}$, minor contributions from $^{12}C^{+}$, $^{26}CN^{-}$, $^{46}NO_2^{-}$, $^{62}NO_3^{-}$, $^{125}H(NO_3)_2^{-}$ (Silva et al., 1999)

Inc., Model 8100) were optimized in order to eliminate transmission of particles with aerodynamic diameters (D_a) below 3 μm. The pull flow of the PCVI was set to 12 vlpm, while the chilled counterflow was set to 6 vlpm. The transmission efficiency (TE) of the PCVI (Figure 3) was determined by passing atomized ammonium sulfate ($(NH_4)_2SO_4$, dried) particles through the PCVI into an APS (TSI 3321). Transmission efficiencies were calculated for particles with diameters larger than 500 nm by determining the ratio of number of particles detected over a 5 minute period without the PCVI to the number of particles detected over a 5 minute period with the PCVI. The TE of particles larger than 3 μm was $5 \times 10^{-3} \pm 11\%$. Particles smaller than 500 nm were not measured due to the lower size limit of the ATOFMS. The ATOFMS-specific TE (described more in section 2.2) is also shown in Figure 3 (green line). Diameters for the 10th, 25th, and 50th percentile (D_{10}, D_{25}, and D_{50}) were calculated using the maximal measured TE (0.05 at 5 μm).

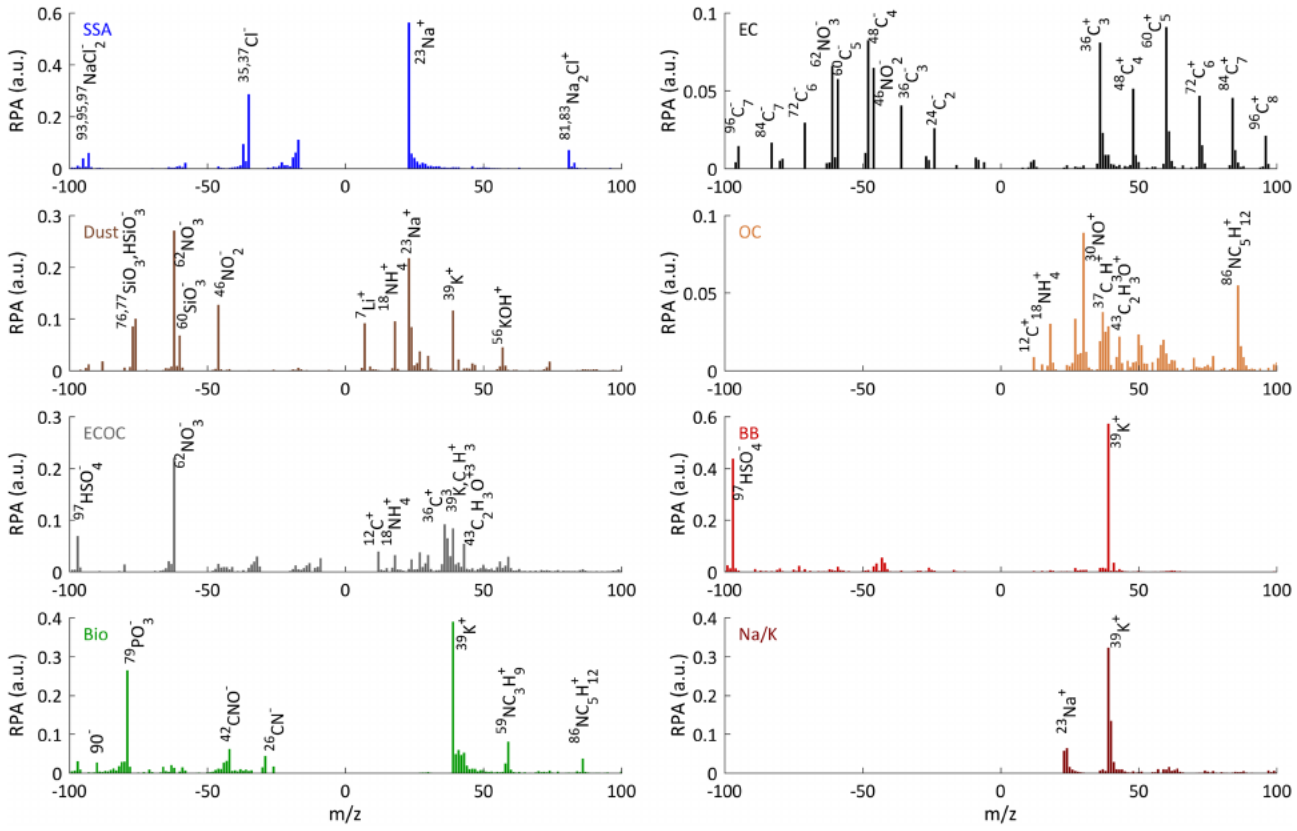

Figure 1. Representative spectra for the ATOFMS particle types observed during this study given in relative peak area (RPA): sea spray aerosol (SSA), dust, elemental carbon organic carbon (ECOC), primary biological (Bio), elemental carbon (EC), organic carbon (OC), biomass burning (BB), and Na/K.

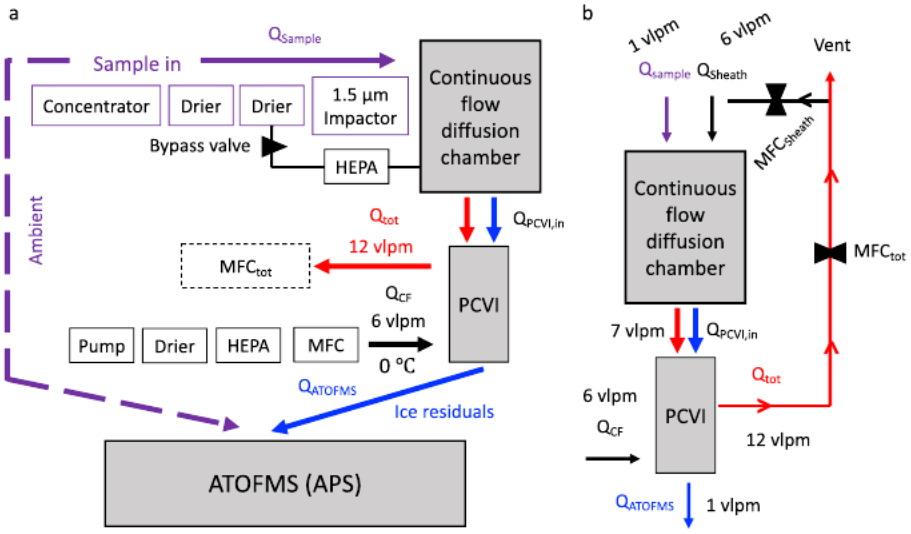

Figure 2. (a) Instrumental setup for the integrated CFDC-PCVI-ATOFMS system. Purple marks samples with both INPs and non-INPs in it. Blue denotes ice crystals while red marks ambient non-INPs. PCVI stands for pumped counterflow virtual impactor. ATOFMS stands for aerosol time-of-flight mass spectrometer, and APS stands for aerodynamic particle sizer. MFC stands for mass flow controller, and HEPA stands for high efficiency particulate air filter. Q_{Sample} Q_{Sheath}, $Q_{PCVI,in}$, Q_{tot}, Q_{CF}, and Q_{ATOFMS} are the flow rates of the sample, sheath, air into the PCVI, total CFDC flow, PCVI counterflow, and ATOFMS flow rate. The purple dashed line shows the instrumental configuration during ambient sampling. (b) Detailed schematic of how flows were controlled during the integrated experiments.

Additional validation experiments were conducted using Arizona Test Dust (ATD) suspended from a fluidized bed and atomized $(NH_4)_2SO_4$. For some of these experiments, aerosol size distributions were measured using an APS. The results of these experiments are detailed in section 3.1.

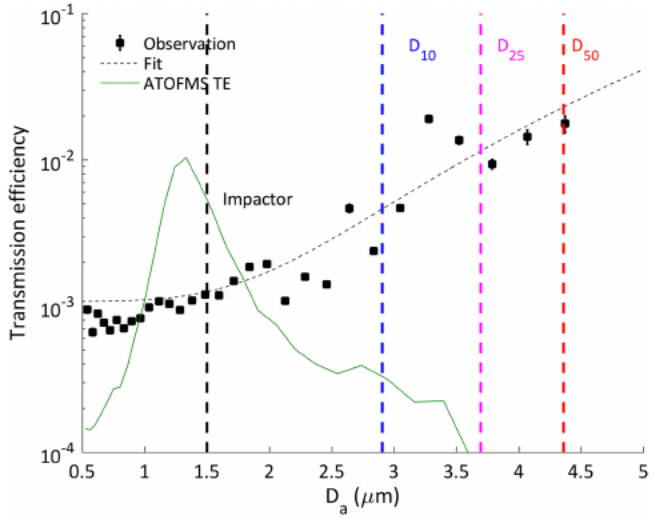

Figure 3. Transmission efficiency curve for the PCVI as a function of aerodynamic diameter (D_a). The green line shows the transmission efficiency for the ATOFMS. Observations are shown in the square markers, while the dashed black line shows the power law fit. The blue, purple, and red dashed lines show the diameters for the 10th, 25th, and 50th percentiles (D_{10}, D_{25}, and D_{50}) of the maximum observed PCVI transmission efficiency. The dark grey dashed line shows the 1.5 μm impactor upstream of the continuous flow diffusion chamber (CFDC).

2.4. Sampling Location and Selection of Control Periods

The CalWater 2015 field campaign was conducted in order to better understand how aerosols interact with landfalling ARs in the Western United States and influence precipitation amount, phase, and spatial distributions (Ralph et al., 2016). As part of this effort, ground-based measurements and air samples were collected from 14 January 2015 to 9 March 2015 at Bodega Marine Laboratory (BML, 38° 19'N, 123° 4') in Bodega Bay, California (Martin et al., 2017). The sampling site at BML included two instrumented trailers located ~100 m ENE of the seashore. Aerosol composition, INP concentrations, and APS size distributions were measured in a trailer operated by the University of California, San Diego (UCSD).

The TE for the ATOFMS was determined via comparison with an APS during ambient sampling at BML. Distributions of ambient aerosol aerodynamic diameter are measured by the APS, and the average number of particles per bin, per unit volume is calculated ($N_{APS,i}$). ATOFMS, size-resolved data are binned using the APS size bins, and the average number of particles per bin (i), per unit volume is calculated ($N_{ATOFMS,i}$). The TE of a given size bin (TE_i) is thus given by

$$TE_i = \frac{N_{ATOFMS,i}}{N_{APS,i}}. \quad (1)$$

Wind speed and direction were determined using a 10 m surface meteorology tower located ~100 m North of the two trailers and operated by the Earth System Research Laboratory, National Oceanic and Atmospheric Administration.

Table 2
Times for Ambient (AMB) and Ice Nucleating Particle Sampling (INP_{-31}) Periods During Operation of the Integrated CFDC-PCVI-ATOFMS System, As well as the Number of Particles Observed by the ATOFMS and CFDC with Positive Spectra

Date	Start time	End time	Sampling type	ATOFMS particles	INP detected by CFDC	Total detection efficiency
12-Feb-2015	21:00:00	23:59:59	AMB	4,730	N/A	N/A
13-Feb-2015	00:14:30	03:12:32	INP_{-31}	25	49,730	6.0×10^{-4}
13-Feb-2015	21:20:54	01:14:02	AMB	2,079	N/A	N/A
14-Feb-2015	01:38:13	03:35:51	INP_{-31}	21	44,379	5.4×10^{-4}
14-Feb-2015	03:48:52	05:20:00	AMB	1,376	N/A	N/A
14-Feb-2015	22:00:00	22:41:18	AMB	995	N/A	N/A
14-Feb-2015	23:11:32	01:23:25	INP_{-31}	11	40,469	3.0×10^{-4}
15-Feb-2015	01:31:57	03:20:00	AMB	2,114	N/A	N/A
15-Feb-2015	20:00:00	21:21:22	AMB	1,632	N/A	N/A
15-Feb-2015	21:24:15	22:56:30	INP_{-31}	4	12,011	3.3×10^{-4}
15-Feb-2015	22:56:30	02:00:00	AMB	1,086	N/A	N/A
16-Feb-2015	18:00:00	19:48:15	AMB	393	N/A	N/A
16-Feb-2015	19:48:16	21:38:12	INP_{-31}	3	20,060	1.5×10^{-4}
16-Feb-2015	21:44:36	00:58:12	AMB	1,169	N/A	N/A
17-Feb-2015	18:00:00	21:00:09	AMB	8,856	N/A	N/A
17-Feb-2015	21:00:00	00:09:47	INP_{-31}	25	43,619	6.0×10^{-4}
18-Feb-2015	00:19:21	03:20:00	AMB	6,060	N/A	N/A
18-Feb-2015	18:50:00	23:36:10	AMB	5,816	N/A	N/A
18-Feb-2015	23:36:10	02:26:29	INP_{-31}	18	67,466	3.3×10^{-4}
19-Feb-2015	2:26:29	05:10:00	AMB	3,008	N/A	N/A

Note. All times are in UTC.

The CFDC-PCVI-ATOFMS system was used to measure the composition of INPs. The CFDC was operated at approximately −31 °C. This temperature is typical of the upper levels (6–10 km) of deep orographic clouds that form over the Sierra Mountains in California (Creamean et al., 2016). Additionally, due to the low sampling efficiency of this system, the CFDC was operated in order to maximize the number of ice crystals created (i.e., at a lower temperature to favor higher INP concentrations). INP composition was measured for a few hours each day, from 12–19 February 2015 (hereafter referred to as the INP_{-31} sampling period). Time periods immediately before and after INP_{-31} sampling were selected for comparison based upon the wind directions and speeds during INP_{-31} sampling, indicating they were of the same air mass (hereafter ambient). Ambient periods totaled 30 hours and 6 minutes, during which the composition of 39,314 individual particles were measured with the ATOFMS. A complete listing of sampling periods can be found in Table 2. Figure 4a shows the time series of wind direction and wind speeds during the INP_{-31} sampling periods (red boxes) and the ambient sampling periods (black boxes). Wind rose plots for the composite sampling periods also show that the conditions were very similar for ambient (Figure 4b) and INP_{-31} (Figure 4c) sampling. It should be noted that from 12 February to 17 February, BML experienced a persistent land/sea breeze pattern, and while the air masses measured here were primarily onshore, they likely contained a moderate influence from terrestrial particles.

2.5. Calculation of Active Site Density

The active site density (n_s expressed here as m^{-2}) for INPs can be expressed as the number concentration of INPs (N_{INP}) per particle surface area per unit volume (S):

$$n_s = \frac{N_{\mathrm{INP}}}{S}. \tag{2}$$

This calculation is typically applied to single INP species, and this approach requires either laboratory studies in which a single particle type can be characterized (Niemand et al., 2012) or ambient air masses dominated by a single particle type such that the n_s can be attributed to one particle type (McCluskey,

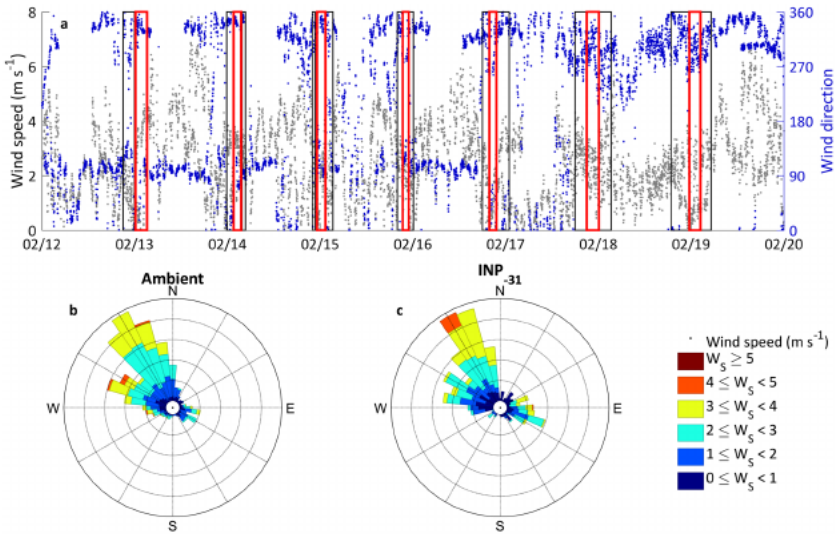

Figure 4. (a) Timeline of wind direction and speed from NOAA/ESRL surface meteorology station. Black boxes indicate ambient sampling periods, while red boxes indicate INP_{-31}. sampling periods. Wind rose for (b) ambient and (c) INP_{-31} sampling periods.

Ovadnevaite, et al., 2018; Price et al., 2018). Neither of these conditions applies to this data set, so we use the integrated CFDC-PCVI-ATOFMS to separate the n_s for dust and SSA. $n_{s,dust}$ and $n_{s,SSA}$ can be defined as the following:

$$n_{s,dust} = \frac{N_{INP,dust}}{S_{dust}} \qquad n_{s,SSA} = \frac{N_{INP,SSA}}{S_{SSA}} \tag{3}$$

In this case, we assume that the number of dust INPs ($N_{INP,dust}$) and SSA INPs ($N_{INP,SSA}$) can be described via the following:

$$N_{INP,dust} = N_{INP} f_{dust} \qquad N_{INP,SSA} = N_{INP} f_{SSA} \tag{4}$$

where N_{INP} is the number concentrations of INPs measured by the CFDC as discussed in section 2.1 and f_{dust} and f_{SSA} are the fraction of INP_{-31} particles measured by the ATOFMS determined to be dust and SSA (see Table 3).

The total surface area (per unit volume) for a given particle class, S_x (i.e., S_{dust} or S_{SSA}), calculated from tandem measurements of the ATOFMS and APS, can be expressed as:

Table 3
Particle Type Number, Fraction, and INP Relative Enhancement Factor (EF)

Particle type	Ambient number	Ambient fraction	INP_{-31} number	INP_{-31} fraction	INP EF
Dust	1,730	0.051	74	0.705	1.000 (0.768–1.232)
Na/K	533	0.016	7	0.067	0.307 (0.156–0.550)
SSA	30,000	0.888	16	0.152	0.013 (0.008–0.019)
Bio	107	0.003	5	0.048	1.093 (0.402–2.183)
EC	616	0.018	1	0.010	0.038 (0.004–0.165)
OC	142	0.004	2	0.019	0.329 (0.087–0.973)
BB	536	0.016	0	0	0 (0–0.106)
ECOC	127	0.004	0	0	0 (0–0.449)

Note. Ambient indicates particles measured during control time periods, and INP_{-31} indicates time periods when ice crystal residuals were measured. Parentheses indicate the 90% confidence intervals.

$$S_x = \sum_{i=1}^{51} D_{p,x,i}^2 \pi \, n_i f_{x,i} \tag{5}$$

where $D_{p,x,i}$ is the particle physical (spherical equivalent) diameter for that bin for particle class x, n_i is the number concentration of particles in that size bin (from measurements made by the APS during INP_{-31} sampling), and $f_{x,i}$ is the fraction of particles of a given particle class (from ambient measurements made by the ATOFMS) for that same size bin. $D_{p,x}$ can be calculated from the aerodynamic diameter, $D_{a,}$ using the following:

$$D_{p,x} = D_a \sqrt{\frac{\rho_o \chi_x}{\rho_x}} \tag{6}$$

where χ is the dynamic shape factor, ρ_0 is the reference density (1 in this case), and ρ_x is the particle density. For our calculations, we assumed that dust had a χ_x of 1.25 (Kaaden et al., 2009) and a ρ_x of 2.65 g cm^{-3} (Kanji et al., 2013), SSA had a χ_x of 1.25, and a ρ_x of 2.2 g cm^{-3} (King et al., 2012), while all other particles were calculated using an effective density of 1.35. ATOFMS-measured values of $D_{a,x}$ were calculated from the particle $D_{va,x}$ using the following:

$$D_{a,x} = D_{va} \sqrt{\frac{\chi_x}{\rho_x}} \tag{7}$$

and assuming that the dynamic shape factors for the continuum and free-molecular regime are roughly equal.

While the ATOFMS can have composition-based biases due to matrix effects, these biases are unlikely to affect the calculation of n_s because the comparisons are within individual particle classes. In other words, because the ATOFMS's sensitivity to a specific particle type, x, would affect the calculation of both $N_{INP,x}$ and S_x, this sensitivity can effectively be discounted.

2.6. Uncertainties in Measurements

While using a particle concentrator in tandem with the integrated CFDC-PCVI-ATOFMS system is a powerful tool for measuring INP composition, there are some uncertainties and limitations with this technique. First, particle concentrators do not uniformly concentrate particles. As shown by Tobo et al., (2013), the concentration factors are strongly size dependent for particles with diameters smaller than approximately 1.5 μm and may thus lead to the selective enhancement of INPs in a variable manner at sizes between about 0.5 and 1 μm. The concentrator performance (ICF ranging from 1.2 to 22.9) during this study was also lower than what has been reported previously, for example, ~90 (Suski et al., 2018). In this study, we assume that the size-related effects on aerosol and INP composition due to the concentrator are relatively minor.

Another limitation to this technique is the necessity for larger particles to be removed prior to measurement by the CFDC with the use of an impactor. This is to ensure that large particles are not erroneously counted as INPs or transmitted through the PCVI and potentially resulting in false positives. However, this doubtlessly leads to an undersampling of INPs as over 50% of INPs measured at surface sites may be larger than 1 μm (Santachiara et al., 2010). This is reflected in the difference between ATOFMS size distributions for ambient particles and ice crystal residuals (Figures S2 and S3 in Supporting Information). Therefore, we cannot rule out that we may have been unable to measure contributors to the INP population.

Finally, it should be noted that the ATOFMS, like other single particle mass spectrometers (SPMS), provides qualitative information. This is because the ionization potentials of materials within a particle can be quite different and thus signals from components that are difficult to ionize may be swamped out by signals from substances with lower ionization potentials (Thomson et al., 1997). Additionally, the ATOFMS has a lower size limit of ~200 nm, and thus we may have failed to measure some smaller INPs. However, as shown by DeMott et al., (2010), most INPs are larger than 0.5 μm, and thus the uncertainty due to the ATOFMS detection efficiency is also likely minor.

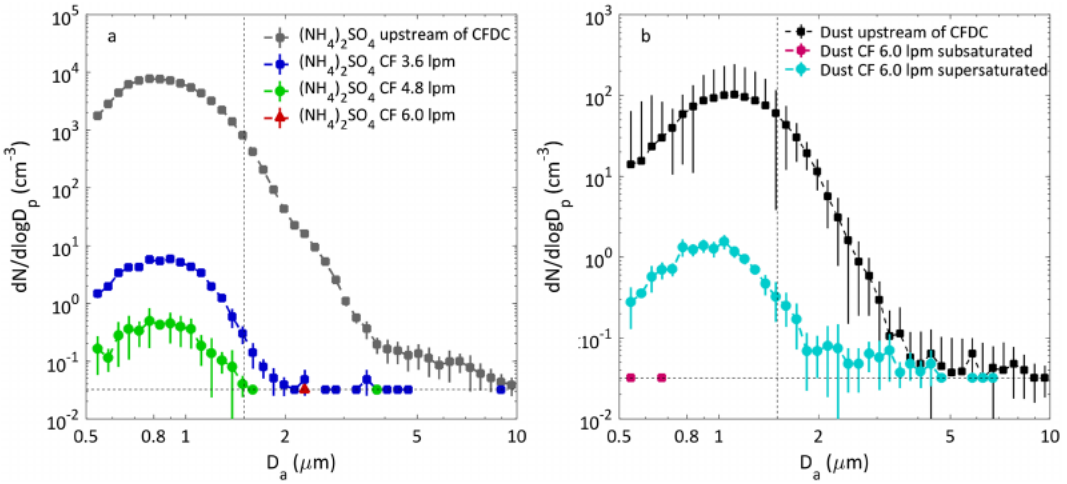

Figure 5. APS number size distributions (dN/dlogD$_p$) measured through the CFDC and PCVI during validation experiments: (a) testing transmission of particles with different counterflows (CF) with $(NH_4)_2SO_4$ and (b) testing transmission of ice crystals formed from ATD in subsaturated and supersaturation conditions. Measurements of controls for both experiments were collected upstream of the CFDC (and its 1.5 μm 50% cut-size impactor, indicated by the vertical dashed line). Error bars indicate the standard deviation. The detection limit of the APS is shown by the horizontal dashed line.

3. Results and Discussion

3.1. Validation of CFDC and ATOFMS Integration

The CFDC-PCVI system was validated by measuring transmission characteristics of a non-INP, $(NH_4)_2SO_4$, and a known IN active material, ATD particles, with an APS (Figure 5). The first set of experiments was conducted using $(NH_4)_2SO_4$ without the CFDC being iced in order to determine transmission of different-sized particles through the PCVI as a function of flow parameters. This was done to optimize flows for assuring PCVI selection of only larger ice particles. Figure 5a shows that for counterflows less than 6.0 vlpm, substantial numbers of $(NH_4)_2SO_4$ particles were measured by the APS at sizes below the desired PCVI cut-point diameter (3 μm). However, at a counterflow of 6.0 vlpm, virtually no particles are transmitted, a sign that the system was working as intended. A second set of experiments using ATD particles was conducted to demonstrate proper transmission of known (activated) INPs with the CFDC set to operational temperature and water supersaturated conditions. The expected reduction or loss of INP activity of ATD at water subsaturation was also examined in proof-of-concept experiments. Figure 5b shows that no particles were detected under subsaturated conditions ($T = -32.8 \pm 0.1$ °C, $SS_w = -18.7 \pm 0.2\%$), while under supersaturated conditions ($T = -32.6 \pm 0.1$ °C, $SS_w = 8.4 \pm 0.4\%$), particles were transmitted through to the APS. It should be noted that particles larger than the upstream impactor (50% cutoff diameter of 1.5 μm) were transmitted through the PCVI under supersaturated conditions. These could be particles that still retained water as the APS was situated immediately after the PCVI with no active method applied to evaporate residual ice. It is unlikely to be large particles not being removed by the upstream impactor because no particles of these sizes were observed under subsaturated conditions.

This second experiment was repeated using the ATOFMS instead of the APS in order to ensure that particle composition could be measured with this instrumental configuration. Figure S1 shows the number of particles detected by the ATOFMS, as well as the number concentrations of total particles greater than 500 nm (N_{500}) and INPs measured by the CFDC (N_{INP}). During this experiment, CFDC chamber temperature was maintained between −27 and −28 °C, while water supersaturation was maintained between 3 and 7% and then later reduced to <0%. Particles were observed by the ATOFMS only when the CFDC was supersaturated (early period in Figure S1) and ice crystals were detected, indicating that the PCVI only transmitted ice crystal residues. A total of 12 particles were measured by the ATOFMS, while the CFDC detected 38,682 INPs during that same time interval, a detection efficiency of 3.10×10^{-4}.

A small percentage of particles below the PCVI cut-point can get through the counterflow, which is known as breakthrough. Due to the scarcity of INPs in the atmosphere, this small amount of breakthrough particles

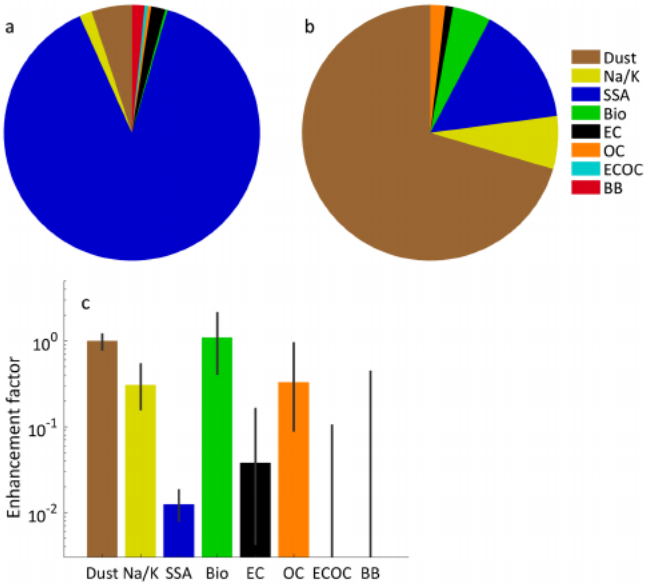

Figure 6. ATOFMS particle type fraction for (a) ambient and (b) INP_{-31}. (c) shows the enhancement factor for each particle type detected during INP_{-31} (see Table 3).

can overwhelm the true INP signal and necessitates an aggressive approach for filtering out particles that are not INPs. A conservative counterflow for the PCVI was used to ensure that non-INPs were eliminated and only ice crystals were transmitted through the PCVI and into the ATOFMS. This conservative approach reduces the probability of false positives from breakthrough of smaller particles but likely contributed to a poor transmission of INPs. Another contributing factor in the poor TE is the TE of the ATOFMS which at its peak is roughly ~1% (seen in Figure 3). As a result of these factors impacting the transmission and detection of INPs, the system is limited to a theoretical INP detection efficiency of $\sim 5 \times 10^{-4}$.

3.2. Ambient and INP_{-31} Composition at Bodega Marine Laboratory

The compositions of ambient particles and ice crystal residuals from the CFDC were measured using ATOFMS at BML (Figure 6). As shown in Figure S3, the impactor upstream of the CFDC greatly affected the size distribution of INP_{-31} measured by the ATOFMS, with ~95% of particles having a D_a below 1.7 μm. Thus, to facilitate the comparison between ambient and INP_{-31} particles, we filtered out ambient particles with D_a larger than 1.7 μm, resulting in the removal of approximately 4,000 particles. 88.8% of the ambient particles were classified as SSA (Figure 6a, Table 3), which was unsurprising due the site's proximity to the Pacific Ocean and onshore flow observed during most of these sampling periods (Figure 4b). The other particle types measured during ambient sampling were dust (5.1%), elemental carbon (EC, 1.8%), Na/K (1.6%), biomass burning (BB, 1.6%), elemental carbon/organic carbon (ECOC, 0.4%), organic carbon (OC, 0.4%), and primary biological (Bio, 0.3%). We note that while it can be difficult to distinguish between fly ash and dust using single particle mass spectrometer (SPMS) measurements, a lack of fly ash sources and the dominant land-sea breeze meteorological pattern (Figure 4) suggests that these particles are overwhelmingly likely to be dust. The Na/K type are particles that were softly desorbed and thus have lower overall $^{23}Na^+$ and $^{39}K^+$ ion intensities. They cannot be assigned to a specific particle type due to the limited number of ion peaks. These results are summarized in Table 3. It should also be noted that the particle-type percentage is partially a reflection of the ATOFMS TE bias toward measuring larger particles (≥0.5 μm) and does not accurately provide the distribution of sources without proper scaling with auxiliary measurements of particle size and mass (Bhave et al., 2002; Qin et al., 2006), as well as the fact that nonspherical particles may be transmitted less efficiently than spherical particles due to particle beam divergence.

The compositions of ice crystal residuals detected by the ATOFMS from all INP_{-31} periods were distinct from the dominant ambient particle types (Figure 6b). Ice crystal residual sampling consisted of a total time of 16 hours and 28 minutes during which the composition of 107 ice crystal residuals was measured. Due to the presence of the impactor upstream of the CFDC, particles smaller than 1.9 μm (the estimated diameter at which 100% of particles are removed by the impactor) were removed from the INP_{-31} analysis. This filtering removed two particles, for a total of 105 ice crystal residuals. During this same time period, 277,734 INPs were detected by the CFDC corresponding to a total detection efficiency of 3.78×10^{-4}, comparable to the detection efficiency from the validation experiments (3.10×10^{-4}; see section 3.1). This detection efficiency is lower than the capture efficiency of the PCVI because the total detection efficiency is also dependent upon the TE of the ATOFMS, which at its peak is ~1% (Figure 3). The most abundant INP particle type was dust which comprised 70.5% of all INP_{-31} particles, while SSA was the second most abundant type at 15.2%. The Na/K (6.7%), Bio (4.8%), EC (1.0%), and OC (1.9%) particle types were minor contributors. Cell fragments and/or biogenic organic compounds are known to be incorporated into aerosol such as dust (Creamean et al., 2013) and SSA (Wang et al., 2015) and have sometimes been described as "biological." However, the Bio-type particles identified at BML in this study are primary biological particles such as bacterial or fungal cells, and these mixed-type particles would be classified as dust or SSA. It should once again be noted that these results are biased toward types in the larger sizes due to the TE of the ATOFMS (see section 2.6 and

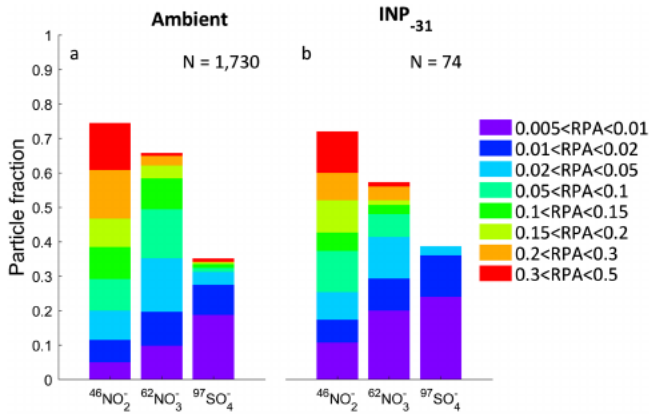

Figure 7. Colorstack plots of nitrate and sulfate ion markers on dust particles for (a) ambient and (b) INP_{-31}. Colored bars indicate the fraction of particles that have a relative peak area (RPA) within the corresponding bounds.

Figures S2 and S3). However, the size range of particles measured in this study (0.5–3.0 μm) overlaps well with the typical size range reported for previous INP size measurements (Kanji et al., 2017). BB and ECOC were not detected during INP_{-31} sampling periods. Previous studies utilizing the CFDC-PCVI-SPMS technique observed particles containing copper and other metals, which were hypothesized to be artifacts originating from either the walls of the CFDC or ice crystal impaction within the PCVI (Cziczo et al., 2003), though we observed no particles containing Cu during this study.

The efficiency with which particles nucleate ice can be determined by comparing the prevalence of a particle type in the ice residuals to their abundance during ambient periods. Here, we define the IN relative enhancement factor (EF) for a particle type using the following relationship:

$$EF = \frac{N_{INP}}{N_{ambient}} \quad (8)$$

where N_{INP} is the fraction of particles for a given type out of all INP particles and $N_{ambient}$ is the fraction of particles for a given type out of all ambient particles. EF values for all types were normalized relative to dust. The particle types with the highest EFs (90% confidence intervals) were the dust and biological types, with 1.000 (0.768–1.232) and 1.093 (0.402–2.183), respectively, while SSA was depleted in ambient aerosol compared to INP_{-31} with an EF of 0.013 (0.008–0.019) (Figure 6c). The high EF values for dust and biological particles are consistent with previous reports of these particle types serving as effective INPs across a range of different temperatures (Atkinson et al., 2013; Boose, Welti, et al., 2016; Garcia et al., 2012; Huffman et al., 2013; Knopf et al., 2011; Niemand et al., 2012; Pratt et al., 2009; Stopelli et al., 2017). The depletion of SSA in ice crystal residuals is also consistent with reports showing that SSA particles have active site densities two to three orders of magnitude lower than mineral and soil dust (DeMott et al., 2016; McCluskey, Ovadnevaite, et al., 2018). In general, the major source of INP_{-31} was identified as mineral dust particles, while the major source in ambient particles was identified as SSA.

The extent, and under which conditions, that atmospheric processing affects immersion mode IN-activity of dust are still uncertain. Lab experiments have shown that treatment with sulfuric acid impairs the IN-activity of dust particles (Augustin-Bauditz et al., 2014; Cziczo et al., 2009; Wex et al., 2014; Sullivan, Petters, et al., 2010; Sullivan, Miñambres, et al., 2010) and has been hypothesized to result from the chemical modification of important surface features on dust particles. In contrast, lab studies of dust aging by nitric acid have showed no impairment of immersion mode IN-activity (Kulkarni et al., 2015; Sullivan, Miñambres, et al., 2010). Field evidence of the effect of particle mixing state upon IN-activity has been more limited. SPMS measurements of dust composition in ice crystal residuals at Storm Peak Laboratory, a high-altitude observatory, were determined to have little sulfate or nitrate present, suggesting that heterogeneous reactions may indeed impair IN-activity of dust particles. The colorstack plots in Figure 7 show the fraction of dust particles (both ambient and INP_{-31}) with relative peak areas (RPAs) ion markers corresponding to nitrate ($^{46}NO_2^-$, $^{62}NO_3^-$) and sulfate ($^{97}HSO_4^-$). For particles of the same type, the RPA for an ion marker qualitatively reflects the amount of that species within a given particle (Cahill et al., 2012). The potential effect of sulfate coatings is difficult to assess in this study due to the minimal presence of sulfate on ambient dust particles. However, there was ample nitrate on both ambient and INP_{-31} dust, implying that nitrate coatings did not impair the immersion mode freezing activity of the measured dust particles.

While SSA may have been a relatively minor source of INPs during this study relative to dust, the ocean may indeed be an important source of INPs, particularly over the remote ocean (Burrows et al., 2013; Vergara-Temprado et al., 2017). SSA are mixtures of inorganic salts, particulate organics (including bacteria and viruses), and organic matter found in the ocean (Cochran, Laskina, et al., 2017; Cochran, Ryder, et al., 2017). ATOFMS ion markers for organic nitrogen and phosphate ($^{26}CN^-$, $^{42}CNO^-$, and $^{79}PO_3^-$) are elevated in SSA with higher amounts of bio-organic species (Lee et al., 2015). The colorstack plots in Figure 8 show

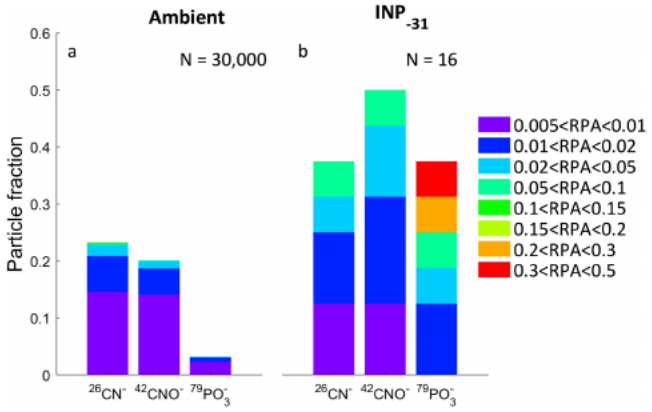

Figure 8. Colorstack plots of organic ion markers for SSA particles for (a) ambient and (b) INP_{-31}. Colored bars indicate the fraction of particles that have a relative peak area (RPA) within the corresponding bounds.

the fraction of SSA particles (both ambient and INP_{-31}) with RPAs for these organic markers. These peaks were significantly elevated in SSA particles detected in ice crystal residuals when compared to ambient SSA. While some caution should be exercised when interpreting these results due to the low number of SSA particles measured during INP_{-31} (16), these results suggest that the organic species in SSA play an important role in their ability to act as INPs. The enrichment of organic markers in SSA measured by the ATOFMS is also consistent with field measurements collected at Mace Head Research Station (McCluskey, Ovadnevaite, et al., 2018) which found elevated organic INPs during a marine transport event. However, we found no evidence (such as mixing with salt species) that the primary biological particles detected in INP_{-31} were oceanic in origin. Interestingly, nearly 12% of dust particles detected in INP_{-31} contained markers indicative of sea salt ($^{81}Na_2Cl^+$ and $^{93}NaCl_2^-$). While we do not currently have a methodology or the capability to distinguish between dust resuspended from the ocean and dust that becomes internally mixed with sea salt through in-cloud processing in the marine boundary layer, this warrants future study.

3.3. Atmospheric Implications

The most striking finding in this study is the prevalence of dust particles serving as INP_{-31}, despite the fact that the majority of ambient aerosols measured by the ATOFMS were SSA. Active site density (n_s) has previously been determined for a number of different particle sources, including mineral dust (Niemand et al., 2012; Ullrich et al., 2017) and SSA (DeMott et al., 2016; McCluskey, Ovadnevaite, et al., 2018). While n_s has also been determined for ambient aerosol where it was deemed that evidence strongly supported a dominance of one particle type (McCluskey, Ovadnevaite, et al., 2018; Price et al., 2018), decomposing the relative contributions to the n_s from different particle sources in an externally mixed aerosol scenario has not been attempted previously. Figure 9 shows the n_s value calculated from the integrated CFDC-PCVI-ATOFMS results (see section 2.5 for more details) for mineral dust (~10^{10} m^{-2}) and SSA (~5×10^8 m^{-2}). Also shown in Figure 9 are parameterizations for dust (N12; Niemand et al., 2012) and SSA (M18; McCluskey, Ovadnevaite, et al., 2018), as well as an exponential fit of n_s values for desert dust dominated air masses (P18; Price et al., 2018). Our results for SSA, $n_{s,SSA}$, are in relatively good agreement with M18, within a factor of 3.0 (evaluated at −31.5 °C, the median temperature for all INP measurements). Our results for dust active site density were within a factor of 3.0 of the N12 parameterization (also evaluated at −31.5 °C). However, N12 was determined in a laboratory setting from a limited selection of dust types and may not accurately represent the ambient dust at Bodega Bay in 2015 due to the importance of both atmospheric aging (Boose, Sierau, et al., 2016; Sullivan, Miñambres, et al., 2010) and mineralogy (Atkinson et al., 2013; Boose, Welti, et al., 2016) for the IN-activity of dust. Figure 9 also shows an exponential fit of n_s of desert-dominated air masses from Price et al. (P18; 2018). The CFDC-PCVI-ATOFMS-derived $n_{s,dust}$ (evaluated at −31.5 °C) is within a factor of 1.6 of the P18 fit. This difference in activity could be due to mineralogy, atmospheric aging, or some combination thereof. DeMott et al. (2015) noted a correction factor for sampling mineral dust INPs to account for the fact that the CFDC may not fully activate these INPs until instrument lamina RH values of up to 109% are used (105% nominal used in this study). DeMott et al. (2015) expressed that it was unclear if similar correction factors would apply to other INP types or to ambient INPs in general. The application of the DeMott et al. (2015) correction factor is indicated in Figure 9 by an upper bar on the data point for mineral dust and shows that the N12

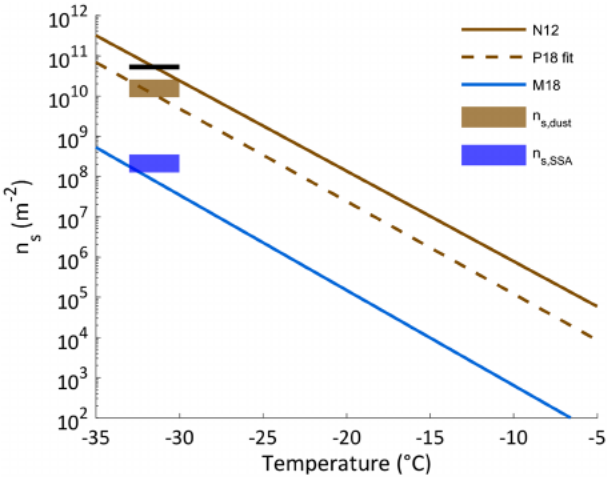

Figure 9. Active site density (n_s) versus temperature for dust (brown) and SSA (blue) as determined by the CFDC-PCVI-ATOFMS. Also shown are n_s parameterizations for dust (N12, brown; Niemand et al., 2012), SSA (M18, blue; McCluskey, Ovadnevaite, et al., 2018), and an exponential fit of dust-dominated air masses (P18, brown dashed line; Price et al., 2018). The application of the DeMott et al. (2015) correction factor is indicated by the black bar above the $n_{s,dust}$ value.

parameterization may better describe the IN-activity of dust. This decomposition of active site densities to their sources highlights the importance of dust in the coastal boundary layer INP population at Bodega Bay during the period of observations in February 2015.

4. Conclusions

The Colorado State University CFDC was integrated with an ATOFMS using a PCVI to directly measure INP composition. Validation experiments confirmed that the ATOFMS only detected particles when the CFDC chamber was producing ice crystals and the typical detection efficiency was 3.10×10^{-4}. The integrated system was deployed to measure INP_{-30} composition at a coastal site in Bodega Bay, California. Ice crystal residuals were enriched with dust particles compared to ambient measurements, which were dominated by SSA. Ice crystal residuals were also comprised of SSA and bioparticles, though in much lower abundance than dust. However, primary bioparticles were also enriched in INP_{-31} relative to ambient, while SSA was not. Dust particles in both ambient and INP_{-31} sampling contained nitrate markers. Lab studies have shown that atmospheric processing by nitric acid does not impair immersion mode freezing (Kulkarni et al., 2015; Sullivan, Petters, et al., 2010), though this is the first time this has been observed in field measurements. SSA particles found in the ice residual samples were found to be enriched in organic species relative to ambient SSA. While the IN-activity of SSA has previously been tied to organic species produced by biological activity in lab (DeMott et al., 2016; McCluskey, Hill, et al., 2018) and field experiments (Creamean et al., 2018; McCluskey, Ovadnevaite, et al., 2018), this is the first time that it has been directly measured in ambient particles. Finally, the active site density (n_s) for dust and SSA particles was calculated using the combined data from the CFDC and ATOFMS. The SSA n_s agreed well with the ambient SSA parameterization from McCluskey, Hill, et al. (2018). The dust n_s may agree better with values estimated from ambient data on dust off Africa (Price et al., 2018), compared to a laboratory-based parameterization (Niemand et al., 2012). The CFDC-PCVI-ATOFMS technique developed and validated in this study illustrates promise for determining the composition and sources of INPs in ambient environments due to its ability to classify individual particles as well as its ability to probe particle mixing state.

Acknowledgments
This research was supported by the Center for Aerosol Impacts on Chemistry of the Environment (CAICE), a National Science Foundation (NSF) Center for Chemical Innovation, and the CalWater 2015 field campaign, funded by the NSF. The authors would also like to thank the UC Davis Bodega Marine Laboratory for the use of laboratory and office space and shipping and physical plant support while collecting data, as well as the California Air Resources Board for the trailer used for sampling. This research was funded by the NSF through award number 1451347 (GC, KP) and award number (1450760, CSM, SMK, PJD). Data are available at https://doi.org/10.6075/J0668BH8.

References

Atkinson, J. D., Murray, B. J., Woodhouse, M. T., Whale, T. F., Baustian, K. J., Carslaw, K. S., et al. (2013). The importance of feldspar for ice nucleation by mineral dust in mixed-phase clouds. *Nature*, *500*(7463), 490–490. https://doi.org/10.1038/nature12384

Augustin-Bauditz, S., Wex, H., Kanter, S., Ebert, M., Niedermeier, D., Stolz, F., et al. (2014). The immersion mode ice nucleation behavior of mineral dusts: A comparison of different pure and surface modified dusts. *Geophysical Research Letters*, *41*, 7375–7382. https://doi.org/10.1002/2014GL061317

Ault, A. P., Williams, C. R., White, A. B., Neiman, P. J., Creamean, J. M., Gaston, C. J., et al. (2011). Detection of Asian dust in California orographic precipitation. *Journal of Geophysical Research*, *116*, 1–15. https://doi.org/10.1029/2010JD015351

Bhave, P. V., Allen, J. O., Morrical, B. D., Fergenson, D. P., Cass, G. R., & Prather, K. a. (2002). A field-based approach for determining ATOFMS instrument sensitivities to ammonium and nitrate. *Environmental Science and Technology*, *36*(22), 4868–4879. https://doi.org/10.1021/es015823i

Bigg, E. K. E. (1973). Ice nucleus concentrations in remote areas. *Journal of the Atmospheric Sciences*, *30*(6), 1153–1157. https://doi.org/10.1016/0169-8095(90)90025-8

Boose, Y., Sierau, B., Isabel García, M., Rodríguez, S., Alastuey, A., Linke, C., et al. (2016). Ice nucleating particles in the Saharan Air Layer. *Atmospheric Chemistry and Physics*, *16*, 9067–9087. https://doi.org/10.5194/acp-16-9067-2016

Boose, Y., Welti, A., Atkinson, J., Ramelli, F., Danielczok, A., Bingemer, H. G., et al. (2016). Heterogeneous ice nucleation on dust particles sourced from nine deserts worldwide - Part 1: Immersion freezing. *Atmospheric Chemistry and Physics*, *16*, 15,075–15,095. https://doi.org/10.5194/acp-16-15075-2016

Burrows, S. M., Hoose, C., Poschl, U., & Lawrence, M. G. (2013). Ice nuclei in marine air: Biogenic particles or dust? *Atmospheric Chemistry and Physics*, *13*, 245–267. https://doi.org/10.5194/acp-13-245-2013

Cahill, J. F., Suski, K., Seinfeld, J. H., Zaveri, R. a., & Prather, K. a. (2012). The mixing state of carbonaceous aerosol particles in northern and southern California measured during CARES and CalNex 2010. *Atmospheric Chemistry and Physics*, *12*, 10,989–11,002. https://doi.org/10.5194/acp-12-10989-2012

Cochran, R. E., Laskina, O., Trueblood, J. V., Estillore, A. D., Morris, H. S., Jayarathne, T., et al. (2017). Molecular diversity of sea spray aerosol particles: Impact of ocean biology on particle composition and hygroscopicity. *Chem*, *2*, 655–667. https://doi.org/10.1016/j.chempr.2017.03.007

Cochran, R. E., Ryder, O. S., Grassian, V. H., & Prather, K. A. (2017). Sea spray aerosol: The chemical link between the oceans, atmosphere, and climate. *Accounts of Chemical Research*, *50*(3), 599–604. https://doi.org/10.1021/acs.accounts.6b00603

Corbin, J. C., Rehbein, P. J. G., Evans, G. J., & Abbatt, J. P. D. (2012). Combustion particles as ice nuclei in an urban environment: Evidence from single-particle mass spectrometry. *Atmospheric Environment*, *51*, 286–292. https://doi.org/10.1016/j.atmosenv.2012.01.007

Creamean, J. M., Kirpes, R. M., Pratt, K. A., Spada, N. J., Maahn, M., de Boer, G., et al. (2018). Marine and terrestrial influences on ice nucleating particles during continuous springtime measurements in an Arctic oilfield location. *Atmospheric Chemistry and Physics*, *18*, 18,023–18,042. https://doi.org/10.5194/acp-2018-545

Creamean, J. M., Suski, K. J., Rosenfeld, D., Cazorla, A., DeMott, P. J., Sullivan, R. C., et al. (2013). Dust and biological aerosols from the Sahara and Asia influence precipitation in the western U.S. *Science (New York, N.Y.)*, *339*, 1572–1578. https://doi.org/10.1126/science.1227279

Creamean, J. M., White, A. B., Minnis, P., Palikonda, R., Spangenberg, D. A., & Prather, K. A. (2016). The relationships between insoluble precipitation residues, clouds, and precipitation over California's southern Sierra Nevada during winter storms. *Atmospheric Environment*, *140*, 298–310. https://doi.org/10.1016/j.atmosenv.2016.06.016

Cziczo, D. J., DeMott, P. J., Brock, C., Hudson, P. K., Jesse, B., Kreidenweis, S. M., et al. (2003). A method for single particle mass spectrometry of ice nuclei. *Aerosol Science and Technology*, *37*(5), 460–470. https://doi.org/10.1080/02786820300976

Cziczo, D. J., Froyd, K. D., Gallavardin, S. J., Moehler, O., Benz, S., Saathoff, H., & Murphy, D. M. (2009). Deactivation of ice nuclei due to atmospherically relevant surface coatings. *Environmental Research Letters*, *4*(4). https://doi.org/10.1088/1748-9326/4/4/044013

DeMott, P. J., Cziczo, D. J., Prenni, A. J., Murphy, D. M., Kreidenweis, S. M., Thomson, D. S., et al. (2003). Measurements of the concentration and composition of nuclei for cirrus formation. *Proceedings of the National Academy of Sciences*, *100*(25), 14,655–14,660. https://doi.org/10.1073/pnas.2532677100

DeMott, P. J., Hill, T. C. J., McCluskey, C. S., Prather, K. A., Collins, D. B., Sullivan, R. C., et al. (2016). Sea spray aerosol as a unique source of ice nucleating particles. *Proceedings of the National Academy of Sciences*, *113*, 5797–5803. https://doi.org/10.1073/pnas.1514034112

DeMott, P. J., Mason, R. H., McCluskey, C. S., Hill, T. C. J., Perkins, R. J., Desyaterik, Y., et al. (2018). Ice nucleation by particles containing long-chain fatty acids of relevance to freezing by sea spray aerosols. *Environmental Science: Processes and Impacts*, *20*, 1559–1569. https://doi.org/10.1039/c8em00386f

DeMott, P. J., Prenni, A. J., Liu, X., Kreidenweis, S. M., Petters, M. D., Twohy, C. H., et al. (2010). Predicting global atmospheric ice nuclei distributions and their impacts on climate. *Proceedings of the National Academy of Sciences*, *107*(25), 11,217–11,11222. https://doi.org/10.1073/pnas.0910818107

Demott, P. J., Prenni, A. J., McMeeking, G. R., Sullivan, R. C., Petters, M. D., Tobo, Y., et al. (2015). Integrating laboratory and field data to quantify the immersion freezing ice nucleation activity of mineral dust particles. *Atmospheric Chemistry and Physics*, *15*, 393–409. https://doi.org/10.5194/acp-15-393-2015

Dettinger, M. D., Ralph, F. M., Das, T., Neiman, P. J., & Cayan, D. R. (2011). Atmospheric rivers, floods and the water resources of California. *Water*, *3*(2), 445–478. https://doi.org/10.3390/w3020445

Eidhammer, T., DeMott, P. J., Prenni, A. J., Petters, M. D., Twohy, C. H., Rogers, D. C., et al. (2010). Ice initiation by aerosol particles: Measured and predicted ice nuclei concentrations versus measured ice crystal concentrations in an orographic wave cloud. *Journal of the Atmospheric Sciences*, *67*(8), 2417–2436. https://doi.org/10.1175/2010JAS3266.1

Fan, J., Leung, L. R., Demott, P. J., Comstock, J. M., Singh, B., Rosenfeld, D., et al. (2014). Aerosol impacts on California winter clouds and precipitation during Calwater 2011: Local pollution versus long-range transported dust. *Atmospheric Chemistry and Physics*, *14*(1), 81–101. https://doi.org/10.5194/acp-14-81-2014

Fan, J., Leung, L. R., Rosenfeld, D., Demott, P. J., Ruby Leung, L., Rosenfeld, D., & Demott, P. J. (2017). Effects of cloud condensation nuclei and ice nucleating particles on precipitation processes and supercooled liquid in mixed-phase orographic clouds. *Atmospheric Chemistry and Physics*, *17*(2), 1017–1035. https://doi.org/10.5194/acp-17-1017-2017

Fergenson, D. P., Pitesky, M. E., Tobias, H. J., Steele, P. T., Czerwieniec, G. A., Russell, S. C., et al. (2004). Reagentless detection and classification of individual bioaerosol particles in seconds. *Analytical Chemistry*, *76*(2), 373–378. https://doi.org/10.1021/ac034467e

Gallavardin, S. J., Froyd, K. D., Lohmann, U., Moehler, O., Murphy, D. M., & Cziczo, D. J. (2008). Single particle laser mass spectrometry applied to differential ice nucleation experiments at the AIDA chamber. *Aerosol Science and Technology*, *42*(9), 773–791. https://doi.org/10.1080/02786820802339538

Garcia, E., Hill, T. C. J., Prenni, A. J., DeMott, P. J., Franc, G. D., & Kreidenweis, S. M. (2012). Biogenic ice nuclei in boundary layer air over two U.S. high plains agricultural regions. *Journal of Geophysical Research*, *117*, 1–12. https://doi.org/10.1029/2012JD018343

Gard, E., Mayer, J. E., Morrical, B. D., Dienes, T., Fergenson, D. P., & Prather, K. A. (1997). Real-time analysis of individual atmospheric aerosol particles: Design and performance of a portable ATOFMS. *Analytical Chemistry*, *69*(20), 4083–4091. https://doi.org/10.1021/ac970540n

Gard, E. E., Kleeman, M. J., Gross, D. S., Hughes, L. S., Allen, J. O., Morrical, B. D., et al. (1998). Direct observation of heterogeneous chemistry in the atmosphere. *Science*, *279*(5354), 1184–1187. https://doi.org/10.1126/science.279.5354.1184

Huffman, J. A., Prenni, A. J., Demott, P. J., Pöhlker, C., Mason, R. H., Robinson, N. H., et al. (2013). High concentrations of biological aerosol particles and ice nuclei during and after rain. *Atmospheric Chemistry and Physics*, *13*, 6151–6164. https://doi.org/10.5194/acp-13-6151-2013

Irish, V. E., Hanna, S. J., Willis, M. D., China, S., Thomas, J. L., Wentzell, J. J. B., et al. (2019). Ice nucleating particles in the marine boundary layer in the Canadian Arctic during summer 2014. *Atmospheric Chemistry and Physics*, *19*(2), 1027–1039. https://doi.org/10.5194/acp-19-1027-2019

Kaaden, N., Massling, A., Schladitz, A., Müller, T., Kandler, K., Schütz, L., et al. (2009). State of mixing, shape factor, number size distribution, and hygroscopic growth of the Saharan anthropogenic and mineral dust aerosol at Tinfou, Morocco. *Tellus Series B: Chemical and Physical Meteorology*, *61*(1), 51–63. https://doi.org/10.1111/j.1600-0889.2008.00388.x

Kanji, Z. A., Ladino, L. A., Wex, H., Boose, Y., Burkert-Kohn, M., Cziczo, D. J., & Krämer, M. (2017). Overview of ice nucleating particles. *Meteorological Monographs*, *58*, 1.1–1.33. https://doi.org/10.1175/AMSMONOGRAPHS-D-16-0006.1

Kanji, Z. A., Welti, A., Chou, C., Stetzer, O., & Lohmann, U. (2013). Laboratory studies of immersion and deposition mode ice nucleation of ozone aged mineral dust particles. *Atmospheric Chemistry and Physics*, *13*, 9097–9118. https://doi.org/10.5194/acp-13-9097-2013

King, S. M., Butcher, A. C., Rosenoern, T., Coz, E., Lieke, K. I., De Leeuw, G., et al. (2012). Investigating primary marine aerosol properties: CCN activity of sea salt and mixed inorganic-organic particles. *Environmental Science and Technology*, *46*(19), 10,405–10,412. https://doi.org/10.1021/es300574u

Knopf, D. A., Alpert, P. A., Wang, B., & Aller, J. Y. (2011). Stimulation of ice nucleation by marine diatoms. *Nature Geoscience*, *4*(2), 88–90. https://doi.org/10.1038/ngeo1037

Kulkarni, G., Pekour, M., Afchine, A., Murphy, D. M., & Cziczo, D. J. (2011). Comparison of experimental and numerical studies of the performance characteristics of a pumped counterflow virtual impactor. *Aerosol Science and Technology*, *45*(3), 382–392. https://doi.org/10.1080/02786826.2010.539291

Kulkarni, G., Nandasiri, M., Zelenyuk, A., Beranek, J., Madaan, N., Devaraj, A., et al. (2015). Effects of crystallographic properties on the ice nucleation properties of volcanic ash particles. *Geophysical Research Letters*, *42*, 3048–3055. https://doi.org/10.1002/2015gl063270

Lee, C., Sultana, C. M., Collins, D. B., Santander, M. V., Axson, J. L., Malfatti, F., et al. (2015). Advancing model systems for fundamental laboratory studies of sea spray aerosol using the microbial loop. *Journal of Physical Chemistry A*, *119*(33), 8860–8870. https://doi.org/10.1021/acs.jpca.5b03488

Martin, A. C., Cornwell, G. C., Atwood, S. A., Moore, K. A., Rothfuss, N. E., Taylor, H., et al. (2017). Transport of pollution to a remote coastal site during gap flow from California's interior: Impacts on aerosol composition, clouds, and radiative balance. *Atmospheric Chemistry and Physics*, *17*(2), 1491–1509. https://doi.org/10.5194/acp-17-1491-2017

Mason, R. H., Si, M., Li, J., Chou, C., Dickie, R., Toom-Sauntry, D., et al. (2015). Ice nucleating particles at a coastal marine boundary layer site: Correlations with aerosol type and meteorological conditions. *Atmospheric Chemistry and Physics*, *15*(21), 12,547–12,566. https://doi.org/10.5194/acp-15-12547-2015

McCluskey, C. S., Hill, T. C. J., Malfatti, F., Sultana, C. M., Lee, C., Santander, M. V., et al. (2017). A dynamic link between ice nucleating particles released in nascent sea spray aerosol and oceanic biological activity during two mesocosm experiments. *Journal of the Atmospheric Sciences*, *74*, 151–166. https://doi.org/10.1175/JAS-D-16-0087.1

McCluskey, C. S., Hill, T. C. J., Sultana, C. M., Laskina, O., Trueblood, J., Santander, M. V., et al. (2018). A mesocosm double feature: Insights into the chemical make-up of marine ice nucleating particles. *Journal of the Atmospheric Sciences*, *75*(7), 2405–2423. https://doi.org/10.1175/JAS-D-17-0155.1

McCluskey, C. S., Ovadnevaite, J., Rinaldi, M., Atkinson, J., Franco, B., Ceburnis, D., et al. (2018). Marine and terrestrial organic ice nucleating particles in Pristine Marine to continentally-influenced Northeast Atlantic air masses. *Journal of Geophysical Research: Atmospheres*, *123*, 6196–6212. https://doi.org/10.1029/2017JD028033

Moffet, R. C., & Prather, K. A. (2009). In-situ measurements of the mixing state and optical properties of soot with implications for radiative forcing estimates. *Proceedings of the National Academy of Sciences*, *106*(29), 11,872–11,877. https://doi.org/10.1073/pnas.0900040106

Niemand, M., Möhler, O., Vogel, B., Vogel, H., Hoose, C., Connolly, P., et al. (2012). A particle-surface-area-based parameterization of immersion freezing on desert dust particles. *Journal of the Atmospheric Sciences*, *69*, 3077–3092. https://doi.org/10.1175/JAS-D-11-0249.1

Pratt, K. A., DeMott, P. J., French, J. R., Wang, Z., Westphal, D. L., Heymsfield, A. J., et al. (2009). In situ detection of biological particles in cloud ice-crystals. *Nature Geoscience*, *2*(6), 398–401. https://doi.org/10.1038/ngeo521

Pratt, K. A., & Prather, K. A. (2010). Aircraft measurements of vertical profiles of aerosol mixing states. *Journal of Geophysical Research*, *115*, D11305. https://doi.org/10.1029/2009JD013150

Price, H. C., Baustian, K. J., McQuaid, J. B., Blyth, A., Bower, K. N., Choularton, T., et al. (2018). Atmospheric ice-nucleating particles in the dusty tropical Atlantic. *Journal of Geophysical Research: Atmospheres*, *123*, 2175–2193. https://doi.org/10.1002/2017JD027560

Qin, X., Bhave, P. V., & Prather, K. A. (2006). Comparison of two methods for obtaining quantitative mass concentrations from aerosol time-of-flight mass spectrometry measurements. *Analytical Chemistry*, *78*(17), 6169–6178. https://doi.org/10.1021/ac060395q

Qin, X., Pratt, K. a., Shields, L. G., Toner, S. M., & Prather, K. a. (2012). Seasonal comparisons of single-particle chemical mixing state in Riverside, CA. *Atmospheric Environment*, *59*, 587–596. https://doi.org/10.1016/j.atmosenv.2012.05.032

Ralph, F. M., Prather, K. A., Cayan, D., Spackman, J. R., Demott, P., Dettinger, M., et al. (2016). Calwater field studies designed to quantify the roles of atmospheric rivers and aerosols in modulating U.S. West Coast Precipitation in a changing climate. *Bulletin of the American Meteorological Society*, *97*(7), 1209–1228. https://doi.org/10.1175/BAMS-D-14-00043.1

Rebotier, T. P., & Prather, K. A. (2007). Aerosol time-of-flight mass spectrometry data analysis: A benchmark of clustering algorithms. *Analytica Chimica Acta*, *585*(1), 38–54. https://doi.org/10.1016/j.aca.2006.12.009

Richardson, M. S., DeMott, P. J., Kreidenweis, S. M., Cziczo, D. J., Dunlea, E. J., Jimenez, J. L., et al. (2007). Measurements of heterogeneous ice nuclei in the western United States in springtime and their relation to aerosol characteristics. *Journal of Geophysical Research*, *112*, 1–16. https://doi.org/10.1029/2006JD007500

Rogers, D. C. (1988). Development of a continuous flow thermal gradient diffusion chamber for ice nucleation studies. *Atmospheric Research*, *22*(2), 149–181. https://doi.org/10.1016/0169-8095(88)90005-1

Romay, F. J., Roberts, D. L., Marple, V. A., Liu, B. Y. H., & Olson, B. A. (2002). A high-performance aerosol concentrator for biological agent detection. *Aerosol Science and Technology*, *36*(2), 217–226. https://doi.org/10.1080/027868202753504074

Santachiara, G., Di Matteo, L., Prodi, F., & Belosi, F. (2010). Atmospheric particles acting as ice forming nuclei in different size ranges. *Atmospheric Research*, *96*(2–3), 266–272. https://doi.org/10.1016/j.atmosres.2009.08.004

Schill, G. P., Jathar, S. H., Kodros, J. K., Levin, E. J. T., Galang, A. M., Friedman, B., et al. (2016). Ice-nucleating particle emissions from photochemically aged diesel and biodiesel exhaust. *Geophysical Research Letters*, *43*, 5524–5531. https://doi.org/10.1002/2016GL069529

Schnell, R. C., & Vali, G. (1976). Biogenic ice nuclei: Part I. Terrestrial and marine sources. *Journal of the Atmospheric Sciences*, *33*(8), 1554–1564. https://doi.org/10.1175/1520-0469(1976)033<1554:BINPIT>2.0.CO;2

Silva, P., & Prather, K. (2000). Interpretation of mass spectra from organic compounds in aerosol time-of-flight mass spectrometry. *Analytical Chemistry*, *72*(15), 3553–3562. https://doi.org/10.1021/ac9910132

Silva, P. J., Carlin, R. A., & Prather, K. A. (2000). Single particle analysis of suspended soil dust from Southern California. *Atmospheric Environment*, *34*(11), 1811–1820. https://doi.org/10.1016/S1352-2310(99)00338-6

Silva, P. J., Liu, D., Noble, C. A., & Prather, K. A. (1999). Size and chemical characterization of individual particles resulting from biomass burning of local Southern California species. *Environmental Science & Technology*, *33*(18), 3068–3076. https://doi.org/10.1021/es980544p

Song, X. H., Hopke, P. K., Fergenson, D. P., & Prather, K. a. (1999). Classification of single particles analyzed by ATOFMS using an artificial neural network, ART-2A. *Analytical Chemistry*, *71*(4), 860–865. https://doi.org/10.1021/ac9809682

Spencer, M. T., & Prather, K. A. (2006). Using ATOFMS to determine OC/EC mass fractions in particles. *Aerosol Science and Technology*, *40*(8), 585–594. https://doi.org/10.1080/02786820600729138

Stopelli, E., Conen, F., Guilbaud, C., Zopfi, J., Alewell, C., & Morris, C. E. (2017). Ice nucleators, bacterial cells and Pseudomonas syringae in precipitation at Jungfraujoch. *Biogeosciences*, *14*(5), 1189–1196. https://doi.org/10.5194/bg-14-1189-2017

Sullivan, R. C., Guazzotti, S. A., Sodeman, D. A., Tang, Y., Carmichael, G. R., & Prather, K. A. (2007). Mineral dust is a sink for chlorine in the marine boundary layer. *Atmospheric Environment*, *41*(34), 7166–7179. https://doi.org/10.1016/j.atmosenv.2007.05.047

Sullivan, R. C., Miñambres, L., Demott, P. J., Prenni, A. J., Carrico, C. M., Levin, E. J. T., & Kreidenweis, S. M. (2010). Chemical processing does not always impair heterogeneous ice nucleation of mineral dust particles. *Geophysical Research Letters*, *37*, L24805. https://doi.org/10.1029/2010GL045540

Sullivan, R. C., Petters, M. D., DeMott, P. J., Kreidenweis, S. M., Wex, H., Niedermeier, D., et al. (2010). Irreversible loss of ice nucleation active sites in mineral dust particles caused by sulphuric acid condensation. *Atmospheric Chemistry and Physics*, *10*(23), 11,471–11,487. https://doi.org/10.5194/acp-10-11471-2010

Sultana, C. M., Al-Mashat, H., & Prather, K. A. (2017). Expanding single particle mass spectrometer analyses for the identification of microbe signatures in sea spray aerosol. *Analytical Chemistry*, *89*(19), 10,162–10,170. https://doi.org/10.1021/acs.analchem.7b00933

Sultana, C. M., Cornwell, G. C., Rodriguez, P., & Prather, K. A. (2017). FATES: a flexible analysis toolkit for the exploration of single-particle mass spectrometer data. *Atmospheric Measurement Techniques*, *10*(4), 1323–1334. https://doi.org/10.5194/amt-10-1323-2017

Suski, K. J., Hill, T. C. J., Levin, E. J. T., Miller, A., DeMott, P. J., & Kreidenweis, S. M. (2018). Agricultural harvesting emissions of ice-nucleating particles. *Atmospheric Chemistry and Physics*, *18*(18), 13,755–13,771. https://doi.org/10.5194/acp-18-13755-2018

Taylor, J. R. (1997). *An introduction to error analysis: The study of uncertainties in physical measurements* (2nd ed.). Sausalito, CA: University Science Books.

Thomson, D. S., Middlebrook, A. M., & Murphy, D. M. (1997). Thresholds for laser-induced ion formation from aerosols in a vacuum using ultraviolet and vacuum-ultraviolet laser wavelengths. *Aerosol Science and Technology*, *26*(6), 544–559. https://doi.org/10.1080/02786829708965452

Tobo, Y., Prenni, A. J., DeMott, P. J., Huffman, J. A., McCluskey, C. S., Tian, G., et al. (2013). Biological aerosol particles as a key determinant of ice nuclei populations in a forest ecosystem. *Journal of Geophysical Research: Atmospheres*, *118*, 10,100–10,110. https://doi.org/10.1002/jgrd.50801

Ullrich, R., Hoose, C., Möhler, O., Niemand, M., Wagner, R., Höhler, K., et al. (2017). A new ice nucleation active site parameterization for desert dust and soot. *Journal of the Atmospheric Sciences*, *74*(3), 699–717. https://doi.org/10.1175/JAS-D-16-0074.1

Vergara-Temprado, J., Murray, B. J., Wilson, T. W., O'Sullivan, D., Browse, J., Pringle, K. J., et al. (2017). Contribution of feldspar and marine organic aerosols to global ice nucleating particle concentrations. *Atmospheric Chemistry and Physics*, *17*(5), 3637–3658. https://doi.org/10.5194/acp-17-3637-2017

Wang, X., Sultana, C. M., Trueblood, J., Hill, T. C. J., Malfatti, F., Lee, C., et al. (2015). Microbial control of sea spray aerosol composition: A tale of two blooms. *ACS Central Science*, *1*(3), 124–131. https://doi.org/10.1021/acscentsci.5b00148

Wex, H., Demott, P. J., Tobo, Y., Hartmann, S., Rösch, M., Clauss, T., et al. (2014). Kaolinite particles as ice nuclei: Learning from the use of different kaolinite samples and different coatings. *Atmospheric Chemistry and Physics*, *14*(11), 5529–5546. https://doi.org/10.5194/acp-14-5529-2014

Wilson, T. W., Ladino, L. A., Alpert, P. A., Breckels, M. N., Brooks, I. M., Browse, J., et al. (2015). A marine biogenic source of atmospheric ice-nucleating particles. *Nature*, *525*(7568), 234–238. https://doi.org/10.1038/nature14986

Zhu, Y., & Newell, R. E. (1998). A proposed algorithm for moisture fluxes from atmospheric rivers. *Monthly Weather Review*, *126*(3), 725–735. https://doi.org/10.1175/1520-0493(1998)126<0725:APAFMF>2.0.CO;2